Transactions on Modelling and Simulation vol 17, © 1997 WIT Press, www.witpress.com, ISSN 1743-355X

Deformation of viscous drops in flow through sinusoidally constricted capillaries

A. Borhan, M. Hemmat
Department of Chemical Engineering, The Pennsylvania State University, University Park, PA 16802, USA

Abstract

The motion of neutrally-buoyant viscous drop in pressure-driven flow through a sinusoidally constricted capillary is examined at low Reynolds number. In the absence of inertial effects, the boundary integral formulation is used to determine the shape of the drop at various axial positions within the capillary. The position-dependent drop speed and the extra pressure loss due to the presence of the drop are also calculated, and the results for small to moderate drop sizes are reported. The effects of the amplitude of corrugation of the capillary wall on the mobility of the drop and the extra pressure loss are also presented.

1 Introduction

The motion of drops and bubbles through capillaries is of interest in a variety of industrial and technical applications. Much of the earlier interest in this subject was motivated by the suggested analogy between the drop motion and the motion of blood cells in the capillaries. These flow systems also arise in many polymer processing operations (e.g. fiber spinning, film blowing, injection molding). We are interested in this problem as a pore scale model of two-phase flow in porous materials (cf. Olbricht [1]). Early mathematical models of the flow through tortuous channels of a porous medium involved modeling the porous medium as a bundle of capillary tubes. Although a straight cylindrical capillary is a gross oversimplification of the true pore geometry in a porous material, it has served to identify the important parameters affecting the mobility of the dispersed phase in flow through porous media. An improved pore-scale model can be obtained by considering capillaries with variable cross-sectional area, in which lagrangian unsteady motion of drops and bubbles can occur (e.g. Westborg & Hassager [2], Gauglitz & Radke [3], Tsai & Miksis [4]). In particular, a capillary whose cross-sectional area varies periodically in the axial direction presents an improvement over the straight cylindrical capillary model because of its inherent converging/diverging configuration that reproduces some of the essential features of the flow kinematics associated with flow through real pore spaces. Aside from a few exceptions (Olbricht & Leal [5], Martinez & Udell [6], Borhan et al. [7, 8]), previous studies of flow through periodically constricted capillaries have been restricted to single-phase flow. A summary of the results of these studies is provided elsewhere (cf. Hemmat & Borhan [9]).

In this paper, we examine the motion of a neutrally-buoyant drop in pressure-driven flow through a sinusoidally constricted capillary under low Reynolds number conditions. We use the boundary integral method, in conjunction with the detailed velocity and pressure distributions obtained earlier for single-phase flow through the capillary (cf. Hemmat & Borhan [9]), in order to compute the velocity and shape of the drop as a function of the axial position of the drop within the capillary. We also determine the extra pressure loss due to the presence of the drop. Experimental observations of Olbricht and Leal [5], and Hemmat and Borhan [10], indicate that a liquid drop or gas bubble moving through a periodically constricted capillary can experience substantial uniaxial extension and biaxial expansion. Thus, the pressure drop requirement for constant flow rate can vary substantially as the drop moves through such a capillary. The prediction of the pressure drop requirement as a function of the position and shape of the drop is significant, from a practical point of view, since it can indicate the possibility of drop entrapment within an equivalent porous structure when a constant applied pressure gradient drives the flow (as encountered in flow through real pore structures), i.e. capillaries which require a large pressure gradient (relative to that imposed) to squeeze the drop through the constrictions could lead to the retention of the drop upstream of those locations.

2 Problem Statement

Consider the axisymmetric motion of a neutrally buoyant drop of radius κR_0 in pressure-driven flow of another liquid within a periodically constricted capillary whose dimensionless radius varies in the axial direction, z, according to

$$R(z) = 1 + A sin(2\pi z/L) \qquad 0 < A < 1, \tag{1}$$

where A and L represent the dimensionless amplitude and wavelength of corrugation, respectively, and all lengths are made dimensionless with respect to the average capillary radius, R_0. The exterior and interior bulk phases, denoted by Ω and Ω', respectively, are incompressible (with density ρ) and Newtonian with corresponding viscosities μ and $\lambda\mu$, and the entire system is assumed to be isothermal. The surface of the drop is represented by S_d, with its unit normal vector $\mathbf{n}$ directed into Ω. In what follows, all velocities are made dimensionless with $V_0 = Q/\pi R_0^2$, where Q is the specified volumetric flow rate through the capillary, all stresses with $\mu V_0/R_0$, and the time with R_0/V_0.

When the Reynolds number is small so that inertial effects can be neglected, the flow fields in the two phases are governed by the continuity and Stokes equations, which, in dimensionless form can be written as

$$\nabla.\mathbf{u} = 0 \quad ; \quad \nabla^2\mathbf{u} = \nabla p \qquad in \ \Omega . \tag{2}$$

$$\nabla.\mathbf{u}' = 0 \quad ; \quad \lambda\nabla^2\mathbf{u}' = \nabla p' \qquad in \ \Omega' , \tag{3}$$

with $\mathbf{u}$ and p representing the velocity and pressure fields in the suspending fluid, respectively, and all quantities with primes referring to those associated with the drop phase. The periodic nature of drop deformations observed experimentally (cf. Olbricht & Leal [5], Hemmat [11]) suggest the assumption of a quasi-steady drop shape at each axial location, z_0, within a time scale smaller than the convective time scale. Thus, relative to a reference frame fixed at the center of mass of the drop and translating with its position-dependent velocity, $U(z)$, the boundary conditions can be written as

$$\mathbf{u} = u(r, z) - U(z_0)\mathbf{e}_z \qquad \mathbf{x} \in S_i \ or \ S_o , \tag{4}$$

$$\mathbf{u} = -U(z_0)\mathbf{e}_z \qquad \mathbf{x} \in S_t , \tag{5}$$

$$\mathbf{u}(\mathbf{x}) = \mathbf{u}'(\mathbf{x}) \qquad \mathbf{x} \in S_d , \tag{6}$$

$$\mathbf{n}\cdot\mathbf{u}'(\mathbf{x}) = \mathbf{n}\cdot(\frac{d\mathbf{x}}{dt}) \qquad \mathbf{x} \in S_d , \tag{7}$$

$$\mathbf{n}\cdot(\mathbf{\Pi} - \mathbf{\Pi}') = \frac{1}{Ca}\mathbf{n}\nabla_s\cdot\mathbf{n} \qquad \mathbf{x} \in S_d , \tag{8}$$

where $\mathbf{e}_z$ is the unit vector in the axial direction, and r is the radial distance from the capillary centerline. Also, $\mathbf{\Pi}$ and $\mathbf{\Pi}'$ represent the Newtonian stress tensors in Ω and Ω', respectively, and $\nabla_s = (\mathbf{I} - \mathbf{nn})\cdot\nabla$ is the surface gradient operator. The capillary number, $Ca = \mu V_0/\sigma$, is a measure of the ratio of viscous forces tending to deform the drop to interfacial tension forces resisting deformation, with σ denoting the interfacial tension at the surface of the drop. The periodic single-phase flow field $u(r, z)$ appearing in boundary condition (4) was obtained in [9]. The boundary conditions on the surface of the drop include the continuity of velocity, the kinematic condition, and the stress balance, respectively. Conditions (6)–(8) on the surface of the drop do not overspecify the problem, since the quasi-steady shape of the drop is unknown *a priori* and must be determined as part of the solution.

3 Numerical Solution

The boundary integral method takes advantage of the linearity of the Stokes equations to yield the following integral relations (cf. Tanzosh et al. [12], Pozrikidis [13]):

$$\int_{\partial\Omega} \mathbf{u}\,.\,\mathbf{K}\,.\,\mathbf{n}\; dS(\mathbf{y}) - \int_{\partial\Omega} \mathbf{J}\,.\,\mathbf{\Pi}\,.\,\mathbf{n}\; dS(\mathbf{y}) = \begin{cases} \mathbf{u}(\mathbf{x}) \;\; for \;\; \mathbf{x} \in \Omega \\ \frac{1}{2}\mathbf{u}(\mathbf{x}) \;\; for \;\; \mathbf{x} \in \partial\Omega \\ 0 \quad for \;\; \mathbf{x} \in S_d, \Omega' \end{cases}, \tag{9}$$

$$\int_{S_d} \mathbf{J}\,.\,\mathbf{\Pi}'\,.\,\mathbf{n}\; dS(\mathbf{y}) - \int_{S_d} \lambda\mathbf{u}'\,.\,\mathbf{K}\,.\,\mathbf{n}\; dS(\mathbf{y}) = \begin{cases} \lambda\mathbf{u}'(\mathbf{x}) \;\; for \;\; \mathbf{x} \in \Omega' \\ \frac{\lambda}{2}\mathbf{u}'(\mathbf{x}) \;\; for \;\; \mathbf{x} \in S_d \\ 0 \quad for \;\; \mathbf{x} \notin S_d, \Omega' \end{cases}, \tag{10}$$

where $\mathbf{x}$ is a fixed point, $\mathbf{y}$ is a variable point on the domain of integration, and

$$\mathbf{J} = \frac{1}{8\pi}\left[\frac{\mathbf{I}}{|\mathbf{y}-\mathbf{x}|} + \frac{(\mathbf{y}-\mathbf{x})(\mathbf{y}-\mathbf{x})}{|\mathbf{y}-\mathbf{x}|^3}\right] \;\; ; \;\; \mathbf{K} = \frac{-3(\mathbf{y}-\mathbf{x})(\mathbf{y}-\mathbf{x})(\mathbf{y}-\mathbf{x})}{4\pi|\mathbf{y}-\mathbf{x}|^5} .$$

The integration domain, $\partial\Omega$, consists of the surface of the drop, S_d, inflow and outflow planes, S_i and S_o, respectively, and the section of the tube wall bounded by those planes, S_t. The inflow and outflow planes are placed sufficiently far upstream and downstream of the drop, respectively, to satisfy boundary condition (4). It is clear from equations (9) and (10) that the velocity at any point can be obtained from a knowledge of the surface velocity and force distributions on $\partial\Omega$ by evaluating the requisite surface integrals. Combining equations (9) and (10), and using the stress condition (8), leads to the following set of coupled integral equations for the unknown surface velocity and force distributions on $\partial\Omega$:

$$\int_{S_t+S_i+S_o} (\mathbf{u}\,.\,\mathbf{K}\,.\,\mathbf{n} \;-\; \mathbf{J}\,.\,\mathbf{f}\,)\, dS(\mathbf{y}) + (1-\lambda)\int_{S_d} \mathbf{u}\,.\,\mathbf{K}\,.\,\mathbf{n}\; dS(\mathbf{y})$$
$$-\frac{1}{Ca}\int_{S_d} \mathbf{J}\,.\,(\mathbf{n}\nabla_s)\,.\,\mathbf{n}\; dS(\mathbf{y}) = \begin{cases} \frac{(1+\lambda)}{2}\,\mathbf{u}(\mathbf{x}) \qquad for \quad \mathbf{x} \in S_d \\ \\ \frac{1}{2}\mathbf{u}(\mathbf{x}) \qquad for \quad \mathbf{x} \in S_t \end{cases}, \tag{11}$$

where the surface force $\mathbf{f}$ is defined as $\mathbf{f} = \mathbf{\Pi} \cdot \mathbf{n}$. In addition, an overall force balance on Ω leads to

$$\int_{\partial\Omega} \mathbf{f} \, dS(\mathbf{y}) = 0. \tag{12}$$

Equations (11) and (12) comprise a set of vector equations for the unknown surface velocity and force distributions on $\partial\Omega$. Since we are only considering axisymmetric drop shapes, the surface integrals in these equations can be reduced to line integrals by performing the azimuthal integrations (in a cylindrical coordinate system) analytically. Thus, given a drop shape, the solution to the flow problem is reduced to one of determining the surface velocity and force distributions on $\partial\Omega$ by solving these equations.

A standard boundary collocation technique was used to solve the above equations. All integrals in Eq. (11) were approximated using an open Romberg algorithm with quadratic variations of $\mathbf{u}$ and $\mathbf{f}$ over each element. For a given drop shape, the unit normal $\mathbf{n}$ and the curvature $\nabla_s \cdot \mathbf{n}$ in Eq. (11) were calculated from their corresponding expressions in cylindrical coordinates using the cubic spline representations $r = r(s)$ and $z = z(s)$ for the drop profile, where s is the normalized arclength ($0 \leq s \leq 1$) in the meridional plane along the generating curve of S_d. Although the kernels $\mathbf{J}$ and $\mathbf{K}$ are singular when $\mathbf{y} = \mathbf{x}$, the singularities are integrable in the sense of a Cauchy principal value. Hence, the integrals over singular elements were evaluated by subtracting the immediate neighborhood of the singular points from the integration domain, integrating the kernels analytically in that region, and then adding the result to the numerically computed integral over the remainder of the domain. These procedures are similar to those used in other studies of free surface flows using the boundary integral method (e.g. Borhan & Mao [14], Pozrikidis [13]).

Starting with initial guesses for the drop shape, drop speed, and the pressure loss between S_i and S_o, integral equation (11) was solved for the unknown surface velocity and force distributions. Typically, a spherical drop shape and the pressure loss for single-phase flow, or the converged solution from a previous computation, were used to initiate the computations. Subsequently, the overall force balance (Eq. (12)) was used to correct the pressure drop Δp between S_i and S_o, and the kinematic condition (Eq. (7)) was integrated using the explicit Euler method to update the drop shape. Finally, the drop speed was corrected according to the axial displacement of the center of mass of the drop. The iterations were continued until the normal velocity, and its relative change beween two successive iterations, dropped below a specified tolerance (typically 10^{-3}) at all nodes on the surface of the drop.

4 Results and Discussion

We consider the effects of drop size and amplitude of corrugation on the deformation of the drop, the instantaneous drop speed, U, and the extra pressure loss due to the presence of the drop, Δp^+, defined as the difference between the computed pressure drop and that obtained earlier (Hemmat & Borhan [10]) for single-phase flow. In these computations, the values of the capillary number, viscosity ratio, and corrugation wavelength remain fixed at $Ca = 0.1$, $\lambda = 1.0$, and $L = 4.0$, respectively. Figure 1 demonstrates the drop profiles at various axial positions within a sinusoidally constricted capillary for two different drop sizes and corrugation amplitudes. In the capillary with $A = 0.1$, small drops ($\kappa = 0.5$) experience slight deformations from their original spherical shape, while larger drops ($\kappa = 0.7$) assume a more ovoidal shape. In both cases, the deformation seems to be more pronounced as the leading end of the drop enters, or its trailing end leaves, the constriction. A simple comparison between the drop shapes at similar axial positions within the capillaries with different amplitudes of corrugation ($A = 0.1$ and $A = 0.3$) demonstrates the substantial effect of corrugation amplitude on the shape evolution of the drop. When the center of mass of the drop approaches the diverging cross-section of the capillary, its leading end is influenced by the velocity field in the expansion region, which is characterized by smaller axial velocities near the capillary centerline than those in the constriction. Hence, the motion of the leading interface is retarded substantially, resulting in a reduction of the curvature of the leading meniscus. At the same time, the large axial velocities within the constriction increase the mobility of the trailing end of the drop, leading to the flattening of the trailing interface. For both drop sizes, the stronger radial component of the velocity field in the diverging cross-section tends to expand the drops in the radial direction, resulting in shorter drops. On the other hand, when the center of mass of the drop approaches the converging cross-section of the capillary, the leading end of the drop is rapidly carried along by the high-velocity fluid elements near the constriction centerline, while its trailing portion still moves with the low-velocity fluid elements in the expansion. This leads to substantial elongation of the drop within the constriction, with high curvatures developing at its leading interface.

Variations of the extra pressure loss along a wavelength of corrugation are presented in Figure 2 as a function of the axial position of the center of mass of the drop for $\kappa = 0.5$. The value of Δp^+ increases as the drop enters the expansion, and reaches its maximum when the center of mass of the drop reaches the converging cross-section. The large values of Δp^+ persist until the center of mass of the drop passes through the constriction, due to substantial blockage of the capillary as the drop moves into the constriction. Subsequently, the extra pressure loss decreases substantially as the drop approaches the diverging cross-section, and finally achieves its minimum value when the center of mass of the drop passes through the diverging cross-section. This behavior is qualitatively different from that reported by Martinez and Udell [6] for larger drops. Increasing the amplitude of corrugation seems to affect the magnitude, as well as the location, of the maximum Δp^+, while the magnitude and location of the minimum remains nearly unchanged.

The instantaneous velocity of the drop is also shown in Figure 2 as a function of the axial position of the center of mass of the drop. The velocity of the drop at each axial position is affected by the axial velocity of the suspending fluid elements in the vicinity of the capillary axis, as well as the magnitude of the local drag force exerted by the capillary wall on the surface of the drop. For the small to intermediate drop sizes considered here, the dominant effect of the mean axial velocity of the suspending fluid tends to contribute to larger drop speeds as the drop enters the converging cross-section, before the large retarding effect of the capillary wall in the constriction eventually causes a reduction in drop speed. Similarly, as the drop leaves the constriction, the substantial reduction in the mean axial velocity of the suspending fluid further retards the motion of the drop until the minimum drop speed is achieved in the diverging cross-section. As was shown in the single-phase analysis of Hemmat and Borhan [10], increasing the amplitude of corrugation results in a substantial increase in the axial velocity of the centerline fluid elements within the constriction, while causing a slight decrease in the centerline velocity in the expansion. The same trend is observed here for the velocity of the drop as it enters the constriction or leaves the expansion region, which confirms our earlier statement about the dominant effect of the mean velocity of the suspending fluid compared to the retarding effect of the wall for the small drop sizes considered here. It is not difficult to see from Figure 2 that the average drop speed through the capillary is an increasing function of the corrugation amplitude. This is consistent with our experimental observations (cf. Hemmat [11]) of an enhancement in the average drop mobility with increasing amplitude of corrugation.

Acknowledgments

Acknowledgement is made to the donors of the Petroleum Research Fund, administered by the American Chemical Society, for partial support of this research.

References

[1] Olbricht, W. L. Prototypes of multiphase flow in porous media, *Ann.*

Transactions on Modelling and Simulation vol 17, © 1997 WIT Press, www.witpress.com, ISSN 1743-355X

Rev. Fluid Mech., 1996, **28**, 187.

[2] Westborg, H. & Hassager, O. creeping motion of long bubbles and drops in capillary tubes, *J. Colloid Interface Sci.*, 1989, **133**, 135.

[3] Gauglitz, P. A. & Radke, C. J. The dynamics of liquid film breakup in constricted cylindrical capillaries, *J. Colloid Interface Sci.*, 1990, **134**, 14.

[4] Tsai, T. M. & Miksis, M. J. Dynamics of a drop in a constricted capillary tube, *J. Fluid Mech.*, 1994, **274**, 197.

[5] Olbricht, W. L. & Leal, L. G. The creeping motion of immiscible drops through a converging/diverging tube, *J. Fluid Mech.*, 1983, **134**, 329.

[6] Martinez, M. J. & Udell, K. S. Axisymmetric creeping motion of drops through a periodically constricted tube, AIP Conference Proceedings, 1989, **197**, 222.

[7] Borhan, A. & Hemmat, M. Creeping motion of drops through periodically corrugated capillaries, AIChE Annual Meeting, Miami Beach, FL, 1992.

[8] Borhan, A., Hemmat, M. & Pallinti, J. Pressure- and buoyancy-driven motion of drops and bubbles through periodically constricted capillaries, AIChE Annual Meeting, San Francisco, CA, 1994.

[9] Hemmat, M. & Borhan, A. Creeping flow through sinusoidally constricted capillaries, *Phys. Fluids*, 1995, **7**, 2111.

[10] Hemmat, M. & Borhan, A. Buoyancy-driven motion of drops and bubbles in a periodically constricted capillary, *Chem. Eng. Commun.*, 1996, **148–150**, 363.

[11] Hemmat, M. The motion of drops and bubbles through sinusoidally constricted capillaries, Ph.D. thesis, The Pennsylvania State University, 1996.

[12] Tanzosh, J., Manga, M., & Stone, H. A. Boundary element methods for viscous free-surface flow problems: Deformation of single and multiple fluid-fluid interfaces, in Boundary Element Technologies (ed C. A. Brebbia & M. S. Ingber), pp. 19-39, Computational Mechanics Publications and Elsevier Applied Science, Southampton,1992.

[13] Pozrikidis, C. *Boundary Integral and Singularity Methods for Linearized Viscous Flow*, Cambridge University Press, Cambridge, 1992.

[14] Borhan, A. & Mao, C. F. Effect of surfactants on the motion of drops through circular tubes, *Phys. Fluids A*, 1992, **4**, 2628.

Transactions on Modelling and Simulation vol 17, © 1997 WIT Press, www.witpress.com, ISSN 1743-355X

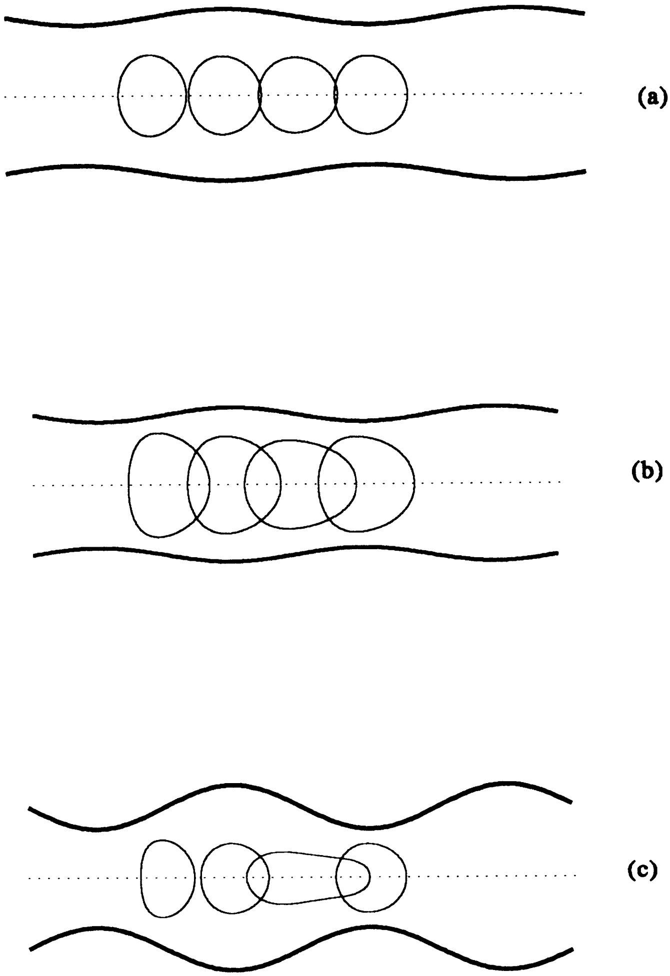

Figure 1. Profiles of a viscous drop at different axial positions in a sinusoidally constricted capillary ;
(a) A = 0.1 , κ = 0.5 ; (b) A = 0.1 , κ = 0.7 ; (c) A = 0.3 , κ = 0.5

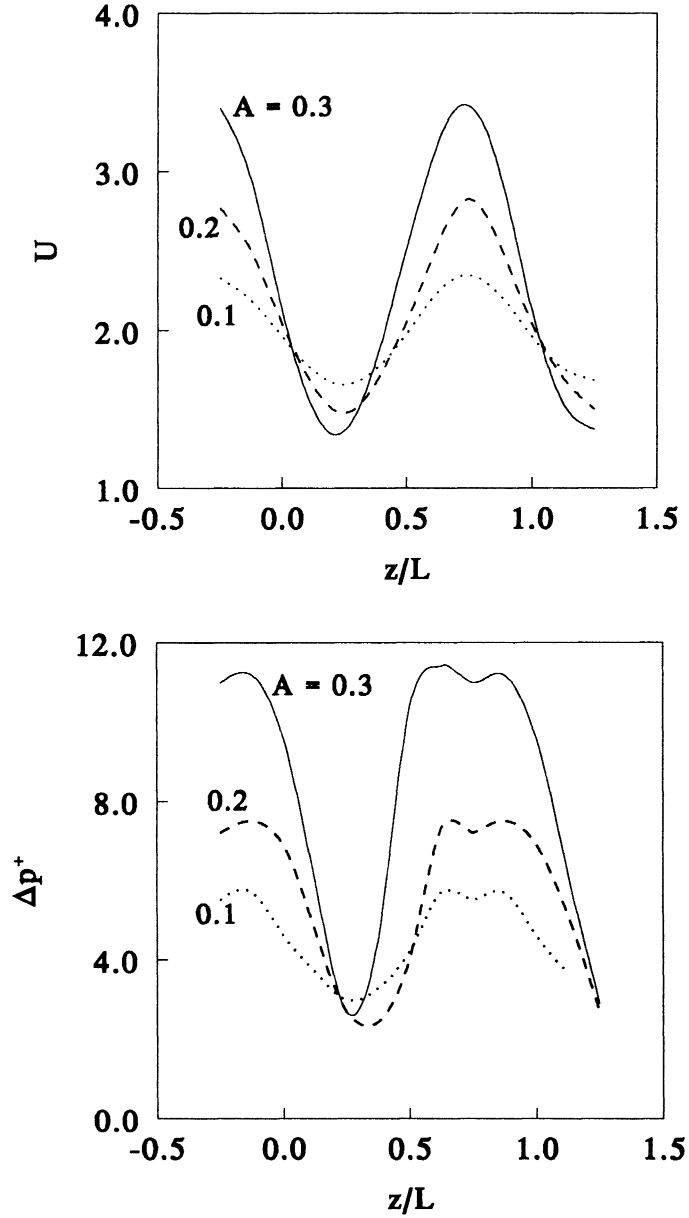

Figure 2. Effect of corrugation amplitude on the drop speed U, and the extra pressure loss Δp^+, for a viscous drop of size $\kappa = 0.5$.